Dalton Transactions

Accepted Manuscript

ROYAL SOCIETY OF CHEMISTRY

www.rsc.org/dalton

Mesoporous $BaTiO_3$@SBA-15 derived via solid state reaction and its excellent adsorption efficiency for the removal of hexavalent chromium from water

Vandana Kumari, Manickam Sasidharan and Asim Bhaumik*

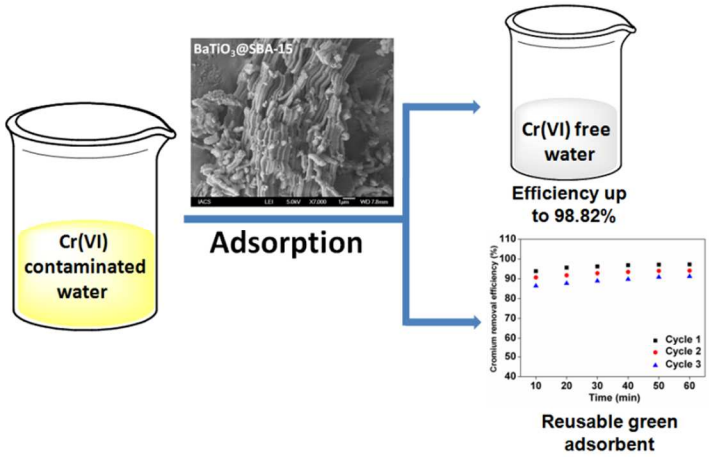

$BaTiO_3$@SBA-15 nanocomposite material has been synthesized via solid state reaction route and it is successfully employed as an adsorbent for the removal of chromium(VI) from contaminated water with very high adsorption efficiency and only 40 min contact time in a batch reactor.

Mesoporous $BaTiO_3$@SBA-15 derived via solid state reaction and its excellent adsorption efficiency for the removal of hexavalent chromium from water

Vandana Kumari,[1] Manickam Sasidharan[2] and Asim Bhaumik*,[1]

[1]*Department of Materials Science, Indian Association for the Cultivation of Science, Jadavpur, Kolkata - 700 032, India*

[2]*SRM Research Institute, SRM University, Kattankulathur, Chennai, 603203, India*

*Address for correspondence. E-mail: msab@iacs.res.in

Abstract

We report the synthesis of barium-titanate/ mesoporous silica nanocomposite material $BaTiO_3$@SBA-15 via aerosol assisted solid state reaction route by using SBA-15 as a hard template. Hexavalent chromium is one of the most harmful contaminants of industrial waste-water. We have used $BaTiO_3$@SBA-15 nanocomposite as an adsorbent for the removal of chromium(VI)-contaminated water and it showed adsorption capacity of 98.2 wt% within only 40 min contact time in a batch reactor. This mesoporous composite has retained this excellent adsorption efficiency for several repetitive cycles for hexavalent chromium, suggesting its future potential for the remediation from water contamination by Cr(VI).

Keywords: $BaTiO_3$ nanoparticles; mesoporous silica; SBA-15; Cr(VI) adsorption; water contamination.

Introduction

The removal of toxic heavy-metal ions/oxyanions of Cr, As, Hg, Pb, Cd, and Cu from the wastewater resources has received a significant attention over the years because of their hazardous nature to the environment and living organisms.[1] Among these one of the most toxic pollutants is hexavalent chromium, which is generated to a large extent due to the industrial chemical processes, tannery,[2] textile industries,[3] chromium electroplating,[4] metal polishing,[5] dye and pigment manufacturing[6] and leather tanning.[7] Chromium exists in the environment in both chromium(III) and chromium(VI) forms. Chromium(III) is an essential microelement for plants, animals and human as it plays an important role in carbohydrate metabolism and nucleic acid synthesis.[8] On the other hand, chromium(VI) is very toxic in nature. Chromium(VI) oxyanions are highly soluble and mobile in aquatic systems. Its long term exposure in drinking water can cause liver damage, pulmonary congestion, severe diarrhoea vomiting, and it is also carcinogenic and mutagenic in living organisms.[9] The maximum allowed level of chromium(VI) in drinking water is 0.05 mg/L according to the standard set by the World Health Organization (WHO).[10] Thus, it has become a primary concern to remove chromium(VI) from industrial effluents before discharging them in to aquatic systems, which could slowly leach into the underground drinking water sources. Various technologies have been employed for the removal of heavy metal ion from industrial wastes like electrocoagulation,[11] electro-chemical precipitation,[12] membrane separation,[13] ion exchange[14] and adsorption.[15] Among them, adsorption is most effective method for waste water treatment, because it is simple and economically favourable. In recent years, a wide variety of adsorbent have been studied including activated carbon,[16] waste biomass,[17] clays, polymer nanofiber[18] and inorganic silicates.[19] Although, these adsorbents showed good removal efficiency for chromium(VI), but these materials have low recyclability, poor efficiency and

their synthesis involved complicated procedures. So it is still a big challenge to design a simple method for high surface area porous nanomaterial with good adsorption capacity, easy separation and regeneration efficiency. Chemical stability and environmental acceptability are the other major concerns, which these adsorbents should satisfy for long term sustainability in the area of water treatment.

In this context, mesoporous materials have attracted widespread interest in many frontier areas of science and technology due to their special characteristic features like exceptionally high surface area, uniform and well–defined pores of nanoscale dimensions.[20] A wide range of mesoporous frameworks composed of metal oxides,[21] sulphides,[22] phosphates,[23] etc. have been invented over last two decades. These materials are utilized for the efficient adsorption of a wide range of cations/anions depending on the surface electrostatic interactions.[24] A variety of functionalized mesoporous polymers have been synthesized, which showed good adsorption efficiency for the toxic inorganic anions present of water.[25] Thus, mesoporous nanocomposite materials, where the presence of the surface positively charged species (metal or metal oxide) could be responsible for the adsorption of contaminant oxyanions present could be a successful strategy for the purification of waste water.[26] Although, there are some reports for the synthesis of mesoporous nanocomposite materials and their use for various adsorption applications, removal of hexavalent chromium from contaminated water still remains a big challenge in the developed world. Various synthetic pathways have been employed for the preparation barium titanate material with different particle sizes and morphologies, such as hydrothermal method,[27] sol-gel technique,[28] solid state route,[29] microwave-hydrothermal process,[30] electrospinning,[31] sol-gel driven hydrothermal method,[32] and solvothermal route.[33]

Herein, we first report the fabrication of low-cost, nontoxic, highly efficient, chemically stable and environment friendly functionalized SBA-15 material ($BaTiO_3$@SBA-15) for the Cr-contaminated treatment. Mesoporous barium titanate/silica nanocomposite has been synthesized via aerosol assisted solid state reaction route by using 2D-hexagonal mesoporous SBA-15 as a high surface area inorganic matrix for the solid support. Detailed characterization of $BaTiO_3$@SBA-15 nanomaterial has been carried out employing powder XRD, N_2 sorption, TEM, SEM, TG-DTA and UV-vis spectroscopic studies. $BaTiO_3$@SBA-15 composite has been successfully employed for the removal of Cr(VI) and detailed adsorption analysis has been conducted to understand the surface interaction between the adsorbent and adsorbate. We strongly believe that due to its high surface area and surface positive charge the $BaTiO_3$@SBA-15 nanomaterials have higher chromium removal efficiency over other $BaTiO_3$ based materials.

Experimental Section:

Starting Materials:

P123 (surfactant), tetraethyl orthosilicate (TEOS, 98%) and titanium isopropoxide (97%) were purchased from Sigma-Aldrich. Barium acetate (AR), 2N HCl, acetic acid and isopropyl alcohol were obtained from Loba Chemie, India. All chemicals were used without any further purification.

Synthesis of amorphous barium-titanate gels:

In a typical synthesis, 2.86 g titanium isopropoxide was taken in a mixture of 15 ml each of isopropyl alcohol and acetic acid. This mixture was stirred for 20 min at 60 ^oC. In a separate beaker 2.54 g barium acetate was dissolved in 5 ml distilled water. The synthetic gel was prepared by very slow addition of the aqueous barium acetate solution to the titanium-isopropoxide solution. The resulting gel was stirred for 5 h at 60 ^oC temperature. After the

complete gelation the semisolid material was kept in a closed polypropylene bottle at 75 ^{o}C for 3 days. Then the content was filtered, washed thoroughly with water and dried under vacuum. The powdered amorphous barium-titanate has been collected by proper grinding of the dried material.

Synthesis of $BaTiO_3$@SBA-15:

The SBA-15 has been synthesized following the reported procedure.[34] For the loading of $BaTiO_3$ nanoparticles at the surface of the mesoporous silica, the amorphous barium-titanate was mixed with template-free mesoporous silica (SBA-15) by grinding it in the mortar together with the addition of a little amount (5 ml) of absolute ethanol. This paste has been filled in calcination boat. The material has been calcined at 700 ^{o}C for 5 h in presence of inert N_2 atmosphere through controlled heating from room temperature at a rate of 5 ^{o}C min^{-1}.

Characterization techniques:

Powder X-ray diffraction patterns of both the as-synthesized and calcined samples were recorded on a Bruker D8 Advance SWAX diffractometer operated at 40 kV voltages and 40 mA current. The instrument has been calibrated with a standard silicon sample, using Ni-filtered Cu K_α (λ = 0.15406 nm) radiation. A JEOL JEM 6700 field emission scanning electron microscope (SEM) was used for the determination of morphology of the nanocomposite material. JEOL JEM 2010 transmission electron microscope operated at an accelerating voltage ranging from 100 kV to 200 kV has been employed for the determination of nanostructure and pore size. Nitrogen adsorption/desorption isotherms were recorded by using a Quantachrome Autosorb 1C surface area analyzer at 77 K. Prior to gas adsorption, samples were degassed for 4 h at 393 K under high vacuum. UV–visible diffuse reflectance spectra were recorded on a Shimadzu UV 2401PC coupled with an integrating sphere attachment. $BaSO_4$ was used as background standard. A

Perkin Elmer differential scanning calorimeter (Diamond DSC7) working under nitrogen atmosphere was used to measure the thermal stability of the mesoporous nanocomposite. The instrument has been calibrated with indium before use. The samples were taken in aluminium pans and were crimped using a universal crimper.

Adsorption analysis:

Adsorption experiments were carried out over mesoporous $BaTiO_3$@SBA-15 materials using aqueous potassium dichromate solutions of known strengths of *ca*. 10–100 ppm as the source of Cr(VI). For the adsorption measurements 0.05 g of $BaTiO_3$@SBA-15 was taken in 20 ml Cr(VI) solution and this solution has been stirred for 1 h at room temperature. Then the adsorbent was removed through filtration. After removing the adsorbent, the initial and final concentration of chromium in these solutions were measured through AAS analysis. We have calculated the percentage removal efficiency of the adsorbent by using following expression:

$$\textbf{Removal efficiency } (\%) = (C_i - C_f)/C_i \times 100$$

Where C_i is the initial concentration and C_f is the final concentration of the chromium ion after treated with $BaTiO_3$-SBA-15 at any time t, respectively.

The effects of the pH on the adsorption of chromium(VI) by mesoporous $BaTiO_3$@SBA-15 were studied by varying the pH of the solutions over the range of 2.0-9.2 by using 0.1 M HCl, 0.1 M NaOH, and 0.1 M CH_3COOH and 0.1 M CH_3COONa aqueous solution. All experiments other than pH study have been carried at pH = 4. In order to determine the adsorption kinetics for the complete removal of chromium(VI) oxyanions, the adsorption experiments are carried out at different times from 0 min to 1 h, at an initial Cr(VI) concentration of 100 ppm and pH=4 at 303 K. The amount of chromium(VI) adsorption at time t, q_t (mg g^{-1}) was calculated by using following expression:

$$q_t = \frac{(C_0 - C_t)V}{W}$$

Where C_0 and C_t (mg L^{-1}) are the concentrations of chromium(VI) initially and at any time t, respectively, V is the volume of the dye solution (L), and W is the mass of adsorbent used (g).

To check the stability of mesoporous $BaTiO_3$-SBA-15, we have collected the adsorbent after experiment and washed with potassium chloride solution to remove the adsorbed chromium (in the form of chromate oxyanion) from the materials, dried and characterized by powder XRD. We have used $BaTiO_3$@SBA-15 for five consecutive cycles for the adsorption of chromium to confirm the reusability and heterogeneous nature of the material.

Results and discussion:

2D-Hexagonal Mesophase:

The small angle powder X-ray diffraction (PXRD) patterns of the calcined SBA-15 and $BaTiO_3$-SBA-15 materials are shown in Figure 1. As seen in Figure 1 SBA-15 shows three characteristic peaks at the 2θ values of 0.88, 1.52 and 1.76, which could be attributed for the 100 (strong), 110 (weak) and 200 (weak) reflections respectively, corresponding to the 2D-hexagonal mesostructure.[20] When the SBA-15 was loaded with the barium-titanate nanoparticles then a considerable decrease in the intensity and shifting in peak positions are observed, however 2D-hexagonal ordering has been retained (Figure 1). The decrease in the intensities and shifting of the peaks reveals that barium-titanate nuclei have been successfully grown at the surface of SBA-15 merial. The wide angle XRD pattern of the barium-titanate immobilized SBA-15 material is shown in Figure 2. This XRD pattern has been indexed and it clearly suggests that the cubic lattice (JCPDS file No. 01-089-2475) type arrangement present in the barium-titanate

nanocrystallities in $BaTiO_3$@SBA-15.[27] Rietveld refinement gives lattice parameters a = 4.015 Å, which is very close to unit cell length of the cubic lattice reported in JCPDS file No. 01-089-2475. In the inset of Figure 2 magnified pattern of the wide angle XRD between 2θ values 43° to 47° of the material is shown. This magnified XRD pattern shows there is no splitting of peak at 45°, which also suggested that the $BaTiO_3$ nanostructure in $BaTiO_3$@SBA-15 have a cubic crystalline phase.[35]

Porosity and Surface Area Analysis:

The Brunauer-Emmett-Telller (BET) surface area and porosity of the mesoporous SBA-15 and $BaTiO_3$@SBA-15 composite nanomaterials are estimated from the respective N_2 adsorption/desorption isotherms at 77 K and these shown in Figure 3 (top and bottom, respectively). Both samples showed typical type IV isotherm, which is characteristic for mesoporous materials together with a very large hysteresis loop (H2 type) in the 0.69 to 0.91 P/P_0 range.[36] The BET surface areas of the pure SBA-15 and $BaTiO_3$@SBA-15 are 771 m^2g^{-1} and 185 m^2g^{-1}, respectively. A considerable decrease in the BET surface area for the $BaTiO_3$@SBA-15 material suggests that barium-titanate nanocrystallites have grown at the pore surface of the 2D-hexagonal mesoporous SBA-15. Corresponding pore size distribution plots of these samples estimated by using the non-local density functional theory (NLDFT)[37] model is shown in the inset of Figure 3. The pore dimension for the SBA-15 was 11.28 nm, which has been distinctly reduced to 9.40 nm after loading of barium-titanate nanocrystallites. The considerable decrease in the pore dimension clearly suggests that barium-titanate nanoparticles have been growth inside the pore channel of the mesoporous SBA-15 material. The calculated pore volume for the mesoporous SBA-15 and material $BaTiO_3$@SBA-15 are 0.9048 and 0.2241 ccg^{-1}, respectively.

Electron microscopic analysis:

Electron microscope images of the mesoporous $BaTiO_3$@SBA-15 are shown in Figure 4. This UHR TEM image of the $BaTiO_3$@SBA-15 suggested that the material have 2D-hexagonal tube like morphology (Figure 4b). The average diameters of the tubes are *ca.* 200-215 nm. The representative TEM images of mesoporous $BaTiO_3$@SBA-15 are shown in Figure 4 (b, c and d). The TEM analysis of the material ($BaTiO_3$@SBA-15) clearly suggests that uniformly ordered mesopores of dimensions *ca*. 8-9 nm have been arranged in a honeycomb like hexagonal array throughout the specimen. The black spots are uniformly distributed throughout the sample and this can be attributed to the presence of $BaTiO_3$ nanoparticles in the mesopores (Figure 4c). The FFT diffractogram shown in the insets of Figure 4c further suggests 2D-hexagonal pore channels. The lattice fringes observed in the HR TEM image of the material $BaTiO_3$@SBA-15 suggested high crystallinity of the material. The distance between two crystal planes (Figure 4d) is quite good agreement with the *d* spacing of (110) crystal plane of cubic crystal structure with unit cell parameter *a*= 4.015 Å (JCPDS file no: 01-089-2475). The corresponding FFT pattern of the $BaTiO_3$@SBA-15 material is shown in the inset of Figure 4d.

UV-visible spectroscopy and Band Gap analysis:

The optical property of the mesoporous $BaTiO_3$@SBA-15 nanomaterial has been evaluated from the UV-visible diffuse reflectance spectroscopy. The UV-visible reflectance spectra of the mesoporous material $BaTiO_3$@SBA-15 are shown in Figure 5. The material shows adsorption maxima at 254 nm, which corresponds to the band gap energy of 3.46 eV (inset of Figure 5). The UV emission of $BaTiO_3$@SBA-15 shows blue shift and has higher bandgap than bulk barium-titanate (3.2 eV). This blue shift in reflectance spectra is good agreement with quantum confinement effects due to decreasing particle size.[38]

Differential scanning calorimetry:

The DSC profile of $BaTiO_3$@SBA-15 in the temperature range 298–793 K is shown in Figure 6. It is pertinent to mention that for cubic $BaTiO_3$ nanomaterial there will be no phase transition and no enthalpy change around 120 ^oC.[39] In Figure 6, the absence of enthalpy peak for $BaTiO_3$@SBA-15 indicates no phase transition around 120 ^oC. This is a good agreement with PXRD pattern at room temperature that the $BaTiO_3$@SBA-15 nanocomposite material is composed of purely cubic crystalline phase.

Adsorption studies: chromium(VI) removal over mesoporous $BaTiO_3$@SBA-15:

The chromium (VI) content in aqueous solutions before and after adsorption studies are given in Table 1. As seen from the Table 1 that $BaTiO_3$@SBA-15 nanocomposite material is very efficient for the removal of Cr(VI) from the aqueous medium than bulk $BaTiO_3$ and pure SBA-15. As we go through the Table 1, the most interesting phenomenon is that with decreasing the concentration of pollutant ion in aqueous medium the efficiency of the $BaTiO_3$ functionalized SBA-15 material increases gradually, which is the most demanding as well as challenging for the purification of waste water in the present scenario of the developed world. $BaTiO_3$@SBA-15 material also showed high distribution coefficient for the removal of chromium(VI) for all these adsorption experiments than the bulk barium-titanate. This could be attributed to the large surface areas and mesoporous architecture of the $BaTiO_3$@SBA-15 material that can interact with chromium(VI) at its surface. Pure silica SBA-15 shows only 3.51% Cr(VI) removal efficiency under identical conditions. The heavy metal ion adsorption at the solid surface is usually based on the electrostatic interaction between the adsorbent and adsorbate.[40] Thus, the surface charge plays an important role in the adsorption phenomena. The surface area and porosity enhances the opportunity for the heavy metals to get adsorbed at the internal surface of

the pores and thus more oxyanions can get adsorbed. For the mesoporous $BaTiO_3$@SBA-15 nanocomposite there is positive charge at its surface due to the oxygen vacancy.[41] Large surface area and positive surface charge are the important factors that can increase the adsorption efficiency of the nanocomposite material towards negatively charged chromate anions (CrO_4^{2-}). We have performed the adsorption experiments in different batches to understand the effect of pH, initial concentration of chromate solutions and adsorption kinetics.

Effect of initial concentration on the adsorption of chromium(VI):

The chromium concentrations in different aqueous solutions before and after treatment with mesoporous $BaTiO_3$@SBA-15 at pH=4.0 are shown in Table 1. As seen from Table 1 that the absorption efficiency for $BaTiO_3$@SBA-15 has been decreases with increasing initial concentrations of chromate solution. For a fixed amount of mesoporous $BaTiO_3$@SBA-15, the total available adsorption sites are limited. This leads to a decrease in removal rate of heavy metals corresponding to an increased initial concentration of chromium oxyanions(VI) in aqueous solutions.[42] We observed that in all these experiments the adsorption efficiency of mesoporous $BaTiO_3$@SBA-15 is more than 97%, thus suggesting that the Cr(VI)-removal rates are not much affected by the initial concentrations of chromium solution.

Effect of pH on chromium(VI) uptake:

The pH of the aqueous solution played an important role in removing of heavy metals and there is an optimum pH for maximum adsorption, below or above which a decrease in uptake generally occurs. The removal of chromium(VI) from aqueous solution over $BaTiO_3$@SBA-15 adsorbent was studied by varying the pH of the solution over the range of 2.0-9.0 for a 100 ppm concentration solution at room temperature. The results are shown in Figure 7. It is observed from the figure that the adsorption of chromium(VI) $BaTiO_3$@SBA-15 increased

with an increase in pH up to 4.0, after that a decrease in the percentage removal efficiency has been observed. The material showed maximum efficiency for the removal of chromium at *ca.* pH = 4.0. Depending upon the pH of solution chromium oxyanions may be exist in solution, as chromate (CrO_4^{2-}), dichromate ($Cr_2O_7^{2-}$) or hydrochromate ($HCrO_4^-$).[43] At lower pH chromium(VI) exists as either $HCrO_4^-$ or $Cr_2O_7^{2-}$, and at higher pH (above about pH = 6), it predominately exists as CrO_4^{2-} ions.[44] Highly acidic conditions (pH 1-2) are not favourable because at lower pH some chromium oxyanions are present in form of undissociated chromate acid ($H_2Cr_2O_7$), which explains the weak adsorption.[45] Furthermore, upon an increase in the pH, adsorption efficiency has been decreased. This may be due to the competition between the increased number of OH^- and chromate oxyanions (CrO_4^{2-}) for adsorption sites. The net positive surface potential of the adsorbent decreases, resulting in a weakening of the electrostatic forces between adsorbent and adsorbate, which ultimately leads to reduction in Cr(VI) removal efficiency.[46] We observed that the adsorption efficiency of mesoporous $BaTiO_3$@SBA-15 for all the Cr(VI) solutions are above 90%, indicating that these removal rates are not much affected by the solution pH. It may be due to the fact that the adsorption of chromium(VI) over mesoporous $BaTiO_3$@SBA-15 is so high that the pH plays a very small role in the removal of chromium(VI).

Adsorption Kinetics:

The effects of adsorption time on the adsorption capacity of chromium(VI) are shown in Figure 8. The result shows that the adsorption capacity of Cr(VI) increases with an increase of adsorption time until equilibrium is reached. The Figure 8 shows that the adsorption rate reaches equilibrium after 40 min. The percentage removal efficiency was found 95.89% in 40 min of contact time. There is no significant change in the equilibrium concentration from 40 min to 60 min. We observed that initially mesoporous $BaTiO_3$-SBA-15 materials adsorb chromium

oxyanions to a large extent. The high uptake of chromium in first 10 minute could be attributed to the multilayer adsorption on the mesoporous surface of $BaTiO_3$-SBA-15. The linear form of the pseudo-second-order kinetic rate model was employed to understand the mechanism of adsorption.[47]

$$\frac{t}{q_t} = \frac{1}{k_2 q_e{}^2} + \frac{t}{q_e}$$

Where k_2 [g/(mg min)] is the rate constant of the pseudo second-order equation and q_t and q_e are the amounts of solute adsorbed on the adsorbent at equilibrium and at time t, respectively. The linear plots of t/q_t versus t are shown in Figure 9. The calculated overall rate constant (k_2) for the material $BaTiO_3$-SBA-15 is 5.168 $x10^{-2}$ g mg^{-1} min^{-1}.

Effect of solution temperature on chromium(VI) adsorption:

The adsorption studies are carried out at three different temperatures 303, 313 and 323 K. The calculated rate constant (k_2) at three different temperatures 303, 313 and 323 K are 5.168 $x10^{-2}$, 5.69 $x10^{-2}$ and 6.32 $x10^{-2}$g mg^{-1} min^{-1} respectively. The results indicate that there is an increase of adsorption capacity with an increase of solution temperature. This may be due to an increase diffusion rate and energy of the adsorbing species, which leads to higher adsorption capacity and faster adsorption rate. These results suggest that the adsorption of Cr(VI) by the $BaTiO_3$@SBA-15 material is endothermic in nature.[48]

Adsorption thermodynamics:

The thermodynamics supposes that in an isolated system, where energy cannot be gained or lost, the entropy change is the driving force.[49] To understand the adsorption thermodynamics for the material $BaTiO_3$-SBA-15 experiments are conducted at different temperatures (303, 313 and 323K). The Arrhenius equation has been used to measure the activation energy of

adsorption,[50] which represents the minimum energy that reactants must have for the reaction to proceed, by using following expression:

$$\ln k_2 = \ln A - \frac{E_a}{RT}$$

R is the gas constant (8.314 J/ mol K), T is the temperature (K), A is the Arrhenius factor and Ea is the Arrhenius activation energy (kJ mol^{-1}). When $\ln k_2$ is plotted against 1/T, a straight line with the slope $-E_a/R$ is obtained (Figure 10). The magnitude of activation energy revels about the type of adsorption such as physical or chemical adsorption. The physisorption processes usually have activation energies in the range of 0–40 $kJmol^{-1}$, while higher activation energies (40–800 $kJmol^{-1}$) suggest chemisorption.[51] The values of the activation energy (8.62 $kJmol^{-1}$) confirm the nature of physisorption processes of $BaTiO_3$@SBA-15 on chromium adsorption.

Reusability of the material:

We have used $BaTiO_3$@SBA-15 for five consecutive cycles for the adsorption of chromium(VI) to confirm reusability and heterogeneous nature of the adsorbent (Figure 11). The adsorbent is recovered from the reaction mixture by filtration. Before the recycling test, the the adsorbent is washed with potassium chloride solution to remove the adsorbed chromium(VI). Then it has been dried overnight at 298 K for 8 h and reused for the next cycle. From Figure 11, it is quite clear that the adsorption efficiency of the material is not much declined after five conjugative cycles, suggesting our mesoporous $BaTiO_3$@SBA-15 can be utilized efficiently for the removal of hexavalent chromium in the long run.

Conclusions

$BaTiO_3$@SBA-15 nanocomposite material has been synthesized via aerosol assisted solid state reaction route by using mesoporous SBA-15 as a hard template. $BaTiO_3$@SBA-15

nanocomposite has been employed as adsorbent for the removal of chromium(VI)-contaminated water. It showed adsorption capacity of 98.2 wt% within only 40 min contact time in a batch reactor and it has retained this excellent adsorption efficiency for several repetitive cycles for hexavalent chromium. Hexavalent chromium being one of the most harmful contaminants of industrial waste-water, this mesoporous nanocomposite material has huge potential for the remediation from water contamination by Cr(VI).

Acknowledgements

VK wishes to thank CSIR, New Delhi for Senior Research Fellowships. AB wishes to thank DST, New Delhi for instrumental supports through the DST Unit on Nanoscience and DST-SERB project grants.

References and Notes:

1 (a) Y. H. Li, J. Ding, Z. Luan, Z. Di, Y. Zhu, C. Xu, D. Wu and B. Wei, *Carbon*, 2003, **41,** 2787–2792; (b) N. H. Hsu, S. L. Wang, Y. C. Lin, G. D. Sheng and J. F. Lee, *Environ. Sci. Technol.,* 2009, **43**, 8801-8806.

2 R. Aravindhan, B. Madhan, J. R. Rao, B. U. Nair and T. Ramsami, *Environ. Sci. Technol.* 2004, **38**, 300–306.

3 Y. Wu, X. Ma, M. Feng and M. Liu, *J. Hazard. Mater.,* 2008, **159,** 380-384.

4 (a) Y. Wang, B. Zou, T. Gao, X. Wu, S. Loua and S. Zhou*, J. Mater. Chem.*, 2012, **22**, 9034-9040; (b) T. Liu, Z. L. Wang, X. Yan and B. Zhang, *Chem. Eng. J.,*2014, **245**, 34-40.

5 V. Sarin, T. S. Singh and K. K. Pant, *Bioresour. Technol.*, 2006, **97**, 1986-1993.

6. A. K. Meena, K. Kadirvelu, G.K. Mishra, Chitra Rajagopal and P. N. Nagar, *J. Hazard. Mater.,* 2008, **150,** 604-611.

7 H. Gu, S. B. Rapole, Y. Huang, D. Cao, Z. Luo, S. Wei and Z. Guo, *J. Mater. Chem. A,* 2013, **1**, 2011-2021.

8 (a) S. L. Lawniczak, P. Lecomte, and J. J. Ehrhardt, *Environ. Sci. Technol.,* 2001, **35**, 1350–1357; (b) Y. Koriche, M. Darder, P. Aranda, S. Semsarib and E. R. Hitzky, *Dalton Trans*., 2014, **43**, 10512-10520.

9 (a) I. Ali, *Chem. Rev.,* 2012, **112**, 5073-5091; (b) P. Miretzky, A. F. Cirelli, *J. Hazard. Mater.,* 2010, **180**, 1-19; (c) D. Mohan, S. Rajput, V. K. Singh, P. H. Steele and C. U. Pittman Jr., *J. Hazard. Mater.,* 2011, **188**, 319-333; (d) N. Sankararamakrishnan, A. Dixit, L. Iyengar and R. Sanghi, *Bioresour. Technol.*, 2006, **97**, 2377-2382; (e) K. Kaya, E. Pehlivan, C. Schmidt and M. Bahadir, *Food Chem.,* 2014, **158**, 112-117.

10 (a) O. Ajouyed, C. Hurel, M. Ammari, L. B. Allal and N. Marmier, *J. Hazard. Mater.,* 2010, **174**, 616–622; (b) L. Dupont and E. Guillon, *Environ. Sci. Technol.,* 2003, **37**, 4235-4241.

11 T. Olmez, *J. Hazard. Mater*., 2009, **162**, 1371-1378.

12 M. Uysal and I. Ar, *J. Hazard. Mater.*, 2007, **149**, 482-491.

13 (a) I. Korus and K. Loska, *Desalination,* 2009, **247**, 390-395; (b) S. Gomes, S. A. Cavaco, M. J. Quina and L. M. G. Ferreira, *Desalination*, 2010, **254**, 80-89; (c) R. K. Goyal, N.S. Jayakumar and M.A. Hashim, *J. Hazard. Mater.*, 2011, **195**, 383-390.

14 (a) Y. Xing, X. Chen and D. Wang, *Environ. Sci. Technol.,* 2007, **41**, 1439–1443;(b) S.K. Sahu, P. Meshram, B.D. Pandey, V. Kumar, T.R. Mankh and, *Hydrometallurgy*, 2009, **99**, 170-174; (c) S. Rengaraj, C. K. Joo, Y. Kim, J. Yi, *J. Hazard. Mater. B*, 2003, **102**, 257–275; (d) S. Edebali, E. Pehlivan, *Chem. Eng. J.*, 2010, **161**, 161-166.

15 (a) Z. Wu and D. Zhao, *Chem. Commun*., 2011, **47**, 3332-3338; (b) D. Zhang, S. Wei, C. Kaila, X. Su, J. Wu, A. B. Karki, D. P. Young and Z. Guo, *Nanoscale*, 2010, **2**, 917-919; (c) Z. Ai, Y. Cheng, L. Zhang, and J. Qiu, *Environ. Sci. Technol.,* 2008**, 42**, 6955–6960; (d) Y. Zhao, J. R. P. Videa, M. L. L. Moreno, M. Ren, G. Saupe, and J. L. G. Torresdey, *Environ. Sci. Technol.*, 2011, **45**, 1082-1087; (e) C. Y. Cao, P. Li, J. Qu, Z. F. Dou, W. S. Yan, J. F. Zhu, Z. Y. Wub and W. G. Song, *J. Mater. Chem.*, 2012, **22**, 19898-19903; (f) H. Wang, N. Yan, Y. Li, X. Zhou, J. Chen, B. Yu, M. Gong and Q. Chen, *J. Mater. Chem.,* 2012, **22**, 9230-9236; (g) B. Liu and Y. Huang, *J. Mater. Chem.,* 2011, **21**, 17413-17418; (h) H. D. Choi, W. S. Jung, J. M. Cho, B. G. Ryu, J. S. Yang, K. Baek, *J. Hazard. Mater. ,* 2009, **166**, 642-646; (i) B. Chen, Z. Zhu, J. Hong, Z. Wen, J. Ma, Y. Qiu and J. Chen, *Dalton Trans.,* 2014, **43**, 10767-10777.

16 (a) M. M. Rao, D. K. Ramana, K. Seshaiah, M. C. Wang and S. W. C. Chien, *J. Hazard. Mater.,* 2009, **166**, 1006-1013; (b) S. Liu, J. Sun and Z. Huang, *J. Hazard. Mater*., 2010, **173**, 377-383; (c) N. K. Hamadi, X. D. Chen, M. M. Farid and M. G. Q. Lu, *Chem. Eng. J.,* 2001, **84**, 95–105; (d) G. Huang, J. X. Shi and T. A. G. Langrish, *Chem. Eng. J.*, 2009, **152**, 434–439; (e) D. Mohan and C. U. Pittman Jr., *J. Hazard. Mater. B,* 2006, **137**, 762–811.

17 (a) V. K. Gupta and S. Sharma, *Environ. Sci. Technol.,* 2002, **36**, 3612–3617; (b) D. Park,

Y. S. Yun, H. Y. Cho and J. M. Park, *Ind. Eng. Chem. Res.,* 2004, **43***,* 8226–8232; (c) L. J. Yu, S. S. Shukla, K. L. Dorris, A. Shukla, J.L. Margrave, *J. Hazard. Mater. B,* 2003, **100**, 53-63; (d) R. Saha and B. Saha, *Desalination Water Treatment*, 2014, **52**, 1928-1936.

18 (a) J. Wang, K. Pan, E. P. Giannelis and B. Cao, *RSC Adv.,* 2013, **3**, 8978-8987; (b) Y. Sang, F. Li, Q. Gu, C. Liang and J. Chen, *Desalination,* 2008, **223**, 349-360.

19 (a) Y. Wang, G. Wang, H. Wang, C. Liang, W. Cai, and L. Zhang, *Chem. Eur. J.,* 2010, **16**, 3497-3503; (b) B. J. Borah and D. K. Dutta, *J. Mol. Catal. A: Chem*., 2013, **366**, 202-209.

20 C. T. Kresge, M. E. Leonowicz, W. J. Roth, J. C. Vartuli and J. S. Beck, *Nature,* 1992, **359**, 710-712.

21 (a) J. B. Joo, Q. Zhang, M. Dahl, I. Lee, J. Goebl, F. Zaera and Y. D. Yin, *Energy Environ. Sci*., 2012, **5**, 6321-6327; (b) R. Y. Zhang, A. A. Elzatahry, S. S. Al-Deyab, and D. Y. Zhao, *Nano Today*, 2012, **7**, 344-366; (c) E. J. W. Crossland, N. Noel, V. Sivaram, T. Leijtens, J. A. Alexander-Webber and H. J. Snaith, *Nature*, 2013, **495**, 215-219.

22 X. P. Fang, X. Q. Yu, S. F. Liao, Y. F. Shi, Y. S. Hu, Z. X. Wang, G. D. Stucky and L. Q. Chen, *Microporous Mesoporous Mater*., 2012, **151**, 418-423.

23 (a) A. Bhaumik and S. Inagaki, *J. Am. Chem. Soc.,* 2001, **123**, 691-696; (b) M. Pramanik, A. K. Patra and A. Bhaumik, *Dalton Trans*., 2013, **42**, 5140-5149.

24 (a) D. Chandra, B. K. Jena, C. R. Raj, and A. Bhaumik, *Chem. Mater.,* 2007**, 19**, 6290-6296; (b) A. Stein, Z. Y. Wang and M. A. Fierke, *Adv. Mater*., 2009, **21**, 265-293; (c) C. Sanchez, P. Belleville, M. Popall and L. Nicole, *Chem. Soc. Rev*., 2011, **40**, 696-753; (d) Y. Wang, X. C. Wang and M. Antonietti, *Angew. Chem. Int. Ed*., 2012, **51**, 68-89.

25 D. Chandra and A. Bhaumik, *J. Mater. Chem.* 2009, **19**, 1901-1907.

26 P. Rudnicki, Z. Hubicki and D. Kolodynska, *Chem. Eng. J*., 2014, **252**, 362-373.

27 (a) P. K. Dutta, R. Asiaie, Sheikh A. Akbar, and W. Zhu, *Chem. Mater., 1994***, *6,*** 1542-1548; (b) Z. Zhou, Y. Lin, H. Tang and H. A Sodano, *Nanotechnol.,* 2013, **24**, 095602.

28 (a) M. R. Mohammadi, D. J. Fray, *Particuology*,2011, **9**, 235–242; (b) F. A. Rabuffetti and R. L. Brutchey, *J. Am. Chem. Soc.,* 2012, **134**, 9475–9487; (c) C. Lemoine, B.Gilbert, B.Michaux, J. P. Pirard and A. J. Lecloux, *J. Non-Crystalline solid.* 1994, **175**, 1-13.

29 E. Brzozowski, M.S. Castro*, J. Eur. Ceram. Soc.,* 2000, **20**, 2347– 2351.

30 E. K. Nyutu, C. H Chen, P. K. Dutta and S. L. Suib, *J. Phys. Chem. C,* 2008, ***112,*** 9659–9667.

31 H. Li, S. Huang, W. Zhang, W. Pan, *J. Alloys Comp.,* 2013, **551**, 131–135.

32 X. Yang, Z. Ren, G. Xu, C. Chao, S. Jiang, S. Deng, G Shen, X. Wei, G. Han, *Ceram. Int.*, 2014, **40**, 9663–9670.

33 Y. V. Kolen'ko, K. A. Kovnir, I. S. Neira, T. Taniguchi, T. Ishigaki, T. Watanabe, N. Sakamoto, and M. Yoshimura, *J. Phys. Chem. C,* 2007, **111**, 7306-7318.

34 J. Q. Wang, L. Huang, M. Xue, Y. Wang, L. Gao, J. H. Zhu, and Z. Zou, *J. Phys. Chem. C.,* 2008, **112**, 5014–5022.

35 (a) I. J. Clark, T. Takeuchi, N. Ohtori and D. C. Sinclair, *J. Mater. Chem.,* 1999, **9**, 83-91; (b) H. Du, S. Wohlrab, M. Weiß and S. Kaskel, *J. Mater. Chem.,* 2007, **17**, 4605-4610.

36 S. K. Das, M. K. Bhunia and A. Bhaumik, *J. Solid State Chem.*, 2010, **183**, 1326-1333.

37 P. I. Ravikovitch and A. V. Neimark, *J. Phys. Chem. B,* 2001**, 105**, 6817–6823.

38 (a) K. Suzuki and K. Kijima, *Jap. J. Appl. Phys.*, 2005, **44**, 2081-2082; (b) W. H. Zhang, J. L. Shi, L. Z. Wang and D. S. Yan, *Chem. Mater.,* 2000**, 12**, 1408-1413; (c) W. Xu, Y.

Liao, and D. L. Akins, *J. Phys. Chem. B,* 2002, **106**, 11127-11131.

39 H. J. Chen and Y. W. Chen, *Ind. Eng. Chem. Res.,* 2003, **42**, 473-483.

40 (a) A. Mahapatra, B. G. Mishra, and G. Hota, *Ind. Eng. Chem. Res*., 2013, **52**, 1554–1561; (b) V. M. Boddu, K.Abburi, J. L. Talbott and E. D. Smith, *Environ. Sci. Technol.,* 2003, **37**, 4449-4456.

41 (a) S. Banerjee, A. Datta, A. Bhaumik and D. Chakravorty, *J. Appl. Phys.*, 2011, **110**, 064316; (b) K. Zagar1, F. H. Ramirez, J. D. Prades, J. R. Morante, A. Recnik and M. Ceh, *Nanotechnol.*, 2011, **22,** 385501.

42 (a) N. N. Fathima, R. Aravindhan, J. R. Rao, and B. U. Nair, *Environ. Sci. Technol.,* 2005, **39**, 2804-2810; (b) K. Selvi, S. Pattabhi, K. Kadirvelu*, Bioresour. Teachnol.*, 2001, **80,** 87-89; (c) S. Kumar and B. C. Meikap, *Desalination Water Treat.,* 2014, **52**, 3122-3132.

43 (a) A. S. K. Kumar, S. Kalidhasan, V. Rajesh, and N. Rajesh, *Ind. Eng. Chem. Res.,* 2012, **51**, 58–69; (b) H.J. Park and L. L. Tavlarides, *Ind. Eng. Chem. Res.,* 2008**, 47**, 3401-3409; (c) S. H. Huang, D. H. Chen, *J. Hazard. Mater.*, 2009, **163**, 174-179.

44 J. H. Chen, H. T. Xing, H. X. Guo, W. Weng, S. R. Hu, S. X. Li, Y. H. Huang, X. Sun and Z. B. Su, *J. Mater. Chem. A,* 2014, **2**, 12561-12570.

45 J. Li, T. Qi, L. Wang, C. Liu and Y. Zhang, *Materials Letters,* 2007, **61**, 3197-3200.

46 (a) H. Jabeen, V. Chandra, S. Jung, J. W. Lee, K. S. Kim and S. B. Kim, *Nanoscale,* 2011, **3**, 3583-3585; (b) A. K. Patra, A. Dutta and A. Bhaumik, *J. Hazard. Mater.*, 2012, **201–202**, 170-177.

47 (a) B.H. Hameed, A.A. Ahmad and N. Aziz, *Chem. Eng. J.,* 2007, **133**, 195-203; (b) Y. S. Ho, *J. Hazard. Mater. B,* 2006, **136**, 681-689.

48 Z.A. A. Othman, R. Ali and M. Naushad, *Chem. Eng. J.*, 2012, **184**, 238-247.

49 K. V. Kumar and A. Kumaran, *Biochem. Eng. J.,* 2005, **27**, 83-93.

50 R. Chen, J. Yu and W. Xiao, *J. Mater. Chem. A,* 2013, **1**, 11682-11690.

51 (a) H. Nollet, M. Roels, P. Lutgen, P. Van Der Meeren and W. Verstraete, *Chemosphere*, 2003, **53**, 655-665; (b) J. J. Fan, W. Q. Cai and J. G. Yu, *Chem. Asian J.*, 2011, **6**, 2481-2490.

Table 1: Adsorption of Cr(VI) over mesoporous $BaTiO_3$@SBA-15 and bulk $BaTiO_3$:

Sample name	Anion content in solution (ppm)		Anion removal efficiency (%)	Distribution coefficient (K_d) (mL/g)[a]
	Before	After		
$BaTiO_3$@SBA -15	100	2.740	97.26	1.4198×10^4
	60	1.458	97.57	1.6060×10^4
	50	1.055	97.89	1.8557×10^4
	40	0.712	98.22	2.2071×10^4
	30	0.471	98.43	2.5077×10^4
	20	0.258	98.71	3.0607×10^4
	10	0.118	98.82	3.3498×10^4
Bulk $BaTiO_3$	100	30.77	69.23	8.998×10^2
	60	15.64	73.92	1.1345×10^3
	50	12.56	74.88	1.1923×10^3
	40	9.744	75.64	1.2420×10^3
	30	7.179	76.07	1.2715×10^3
	20	4.616	76.92	1.3331×10^3
	10	2.292	77.08	1.3452×10^3
Pure SBA-15	100	96.49	3.51	1.455×10^1

[a]Distribution coefficient (K_d) between solid and aqueous phase = number of CrO_4^{2-} adsorbed per g of the solid/number of CrO_4^{2-} present per ml solution after exchange.

$K_d = C_{solid}/C_{water}$ (mol g^{-1}/mol ml^{-1}) = C_{solid}/C_{water} (ml/g).

Figure captions

Figure 1. Small angle powder XRD patterns of (a) pure SBA-15 (b) barium-titanate loaded SBA-15.

Figure 2. Wide angle powder XRD pattern of $BaTiO_3$@SBA-15.

Figure 3. N_2 adsorption (●)-desorption (○) isotherms of the pure SBA-15 (top) and $BaTiO_3$@SBA-15 (down) at 77 K. Corresponding NLDFT pore size distributions are shown in the inset.

Figure 4. FE-SEM image of $BaTiO_3$@SBA-15 (a), UHR TEM image of mesoporous $BaTiO_3$@SBA-15 **(b, c)** (FFT pattern for the hexagonal ordering shown in the inset of figure c), lattice fringes pattern for the $BaTiO_3$ nanoparticle loaded mesoporous SBA-15 **(d)** (FFT pattern for the barium-titanate nanoparticle shown in the inset).

Figure 5. UV-Visible diffuse reflectance of $BaTiO_3$@SBA-15. Bandgap of the material is shown in inset.

Figure 6. DSC profile of the as-synthesized $BaTiO_3$@SBA-15 material.

Figure 7. Effect of pH on the adsorption capacity of Cr(VI) on $BaTiO_3$@SBA-15 material.

Figure 8. The chromium adsorption kinetics of $BaTiO_3$@SBA-15 material as a function of time.

Figure 9. Pseudo-second-order kinetic for adsorption of Cr(VI) on $BaTiO_3$@SBA-15.

Figure 10. Plot of ln k_2 versus 1/T for Cr(VI) adsorption on $BaTiO_3$@SBA-15.

Figure 11. Chromium removal efficiency for several adsorption cycles with time over $BaTiO_3$@SBA-15.

Figure 1 [Kumari, Sasidharan and Bhaumik]

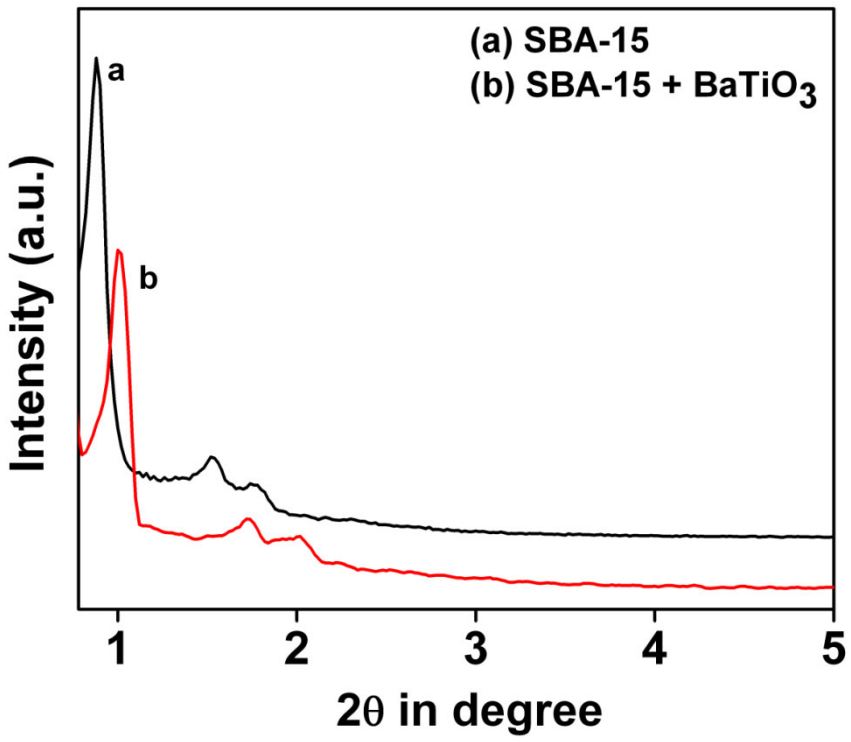

Figure 2 [Kumari, Sasidharan and Bhaumik]

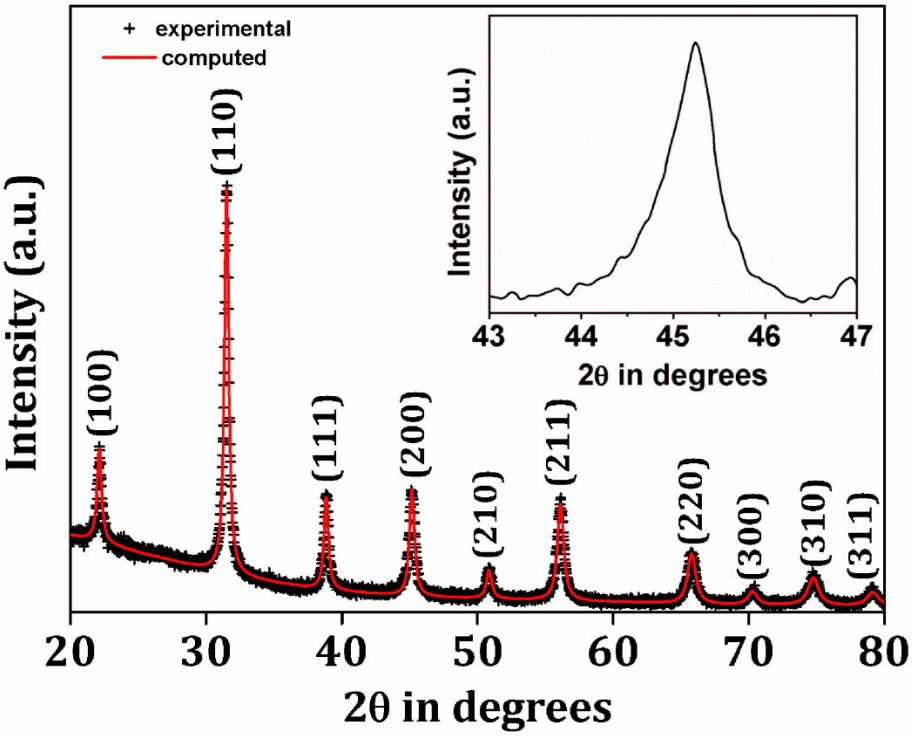

Figure 3 [Kumari, Sasidharan and Bhaumik]

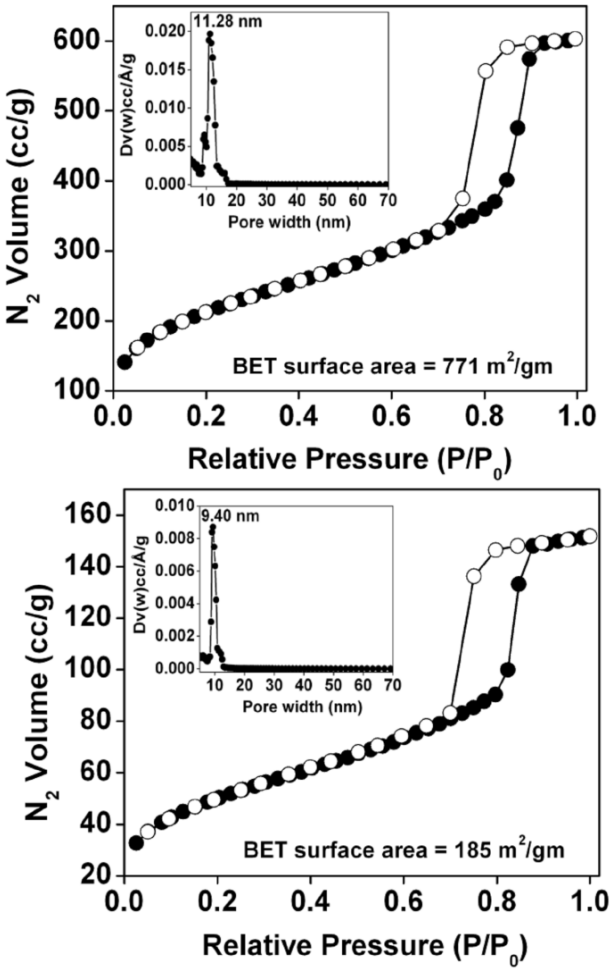

Figure 4 [Kumari, Sasidharan and Bhaumik]

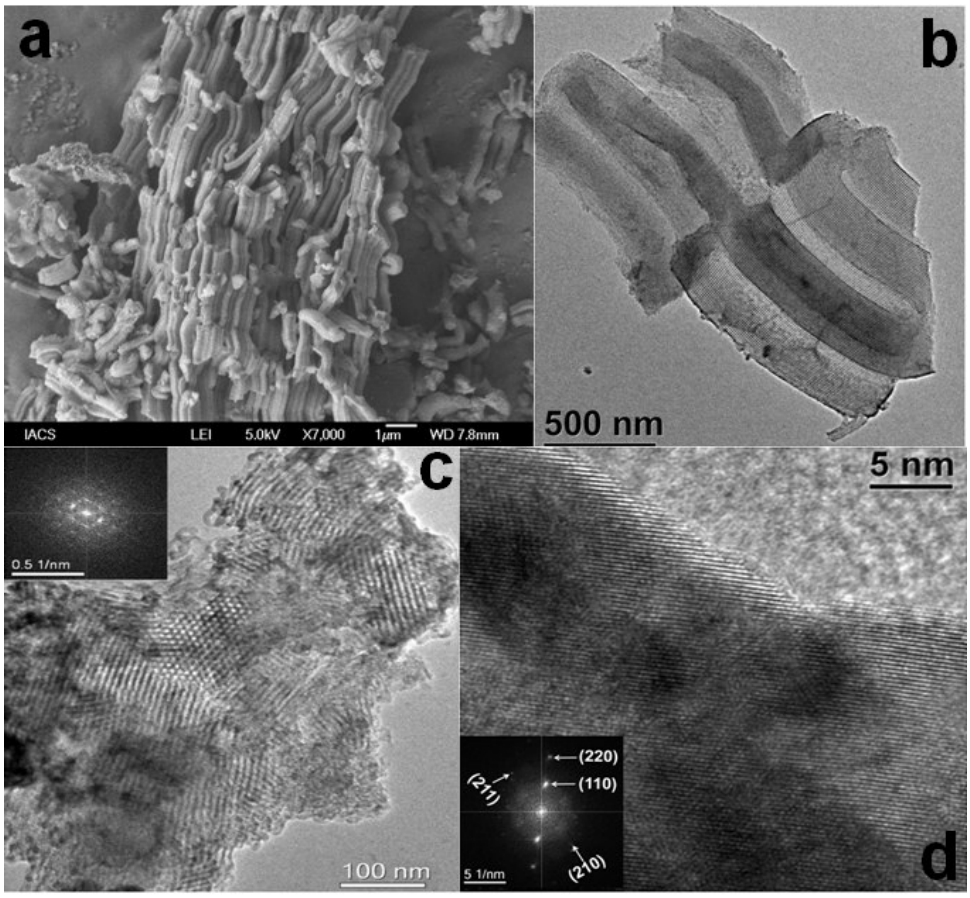

Figure 5 [Kumari, Sasidharan and Bhaumik]

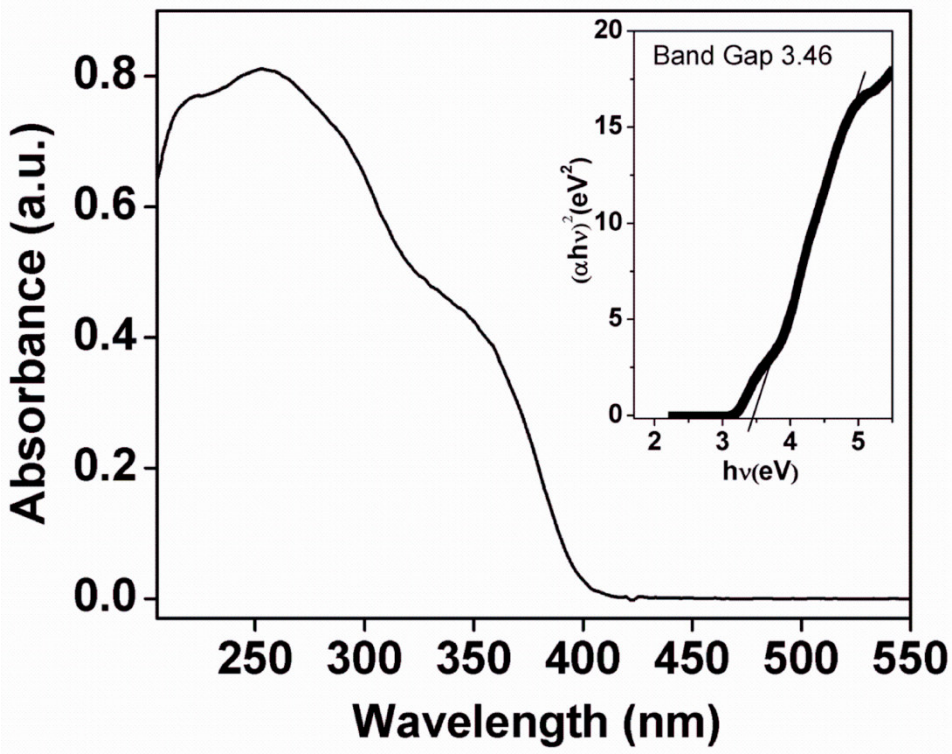

Figure 6 [Kumari, Sasidharan and Bhaumik]

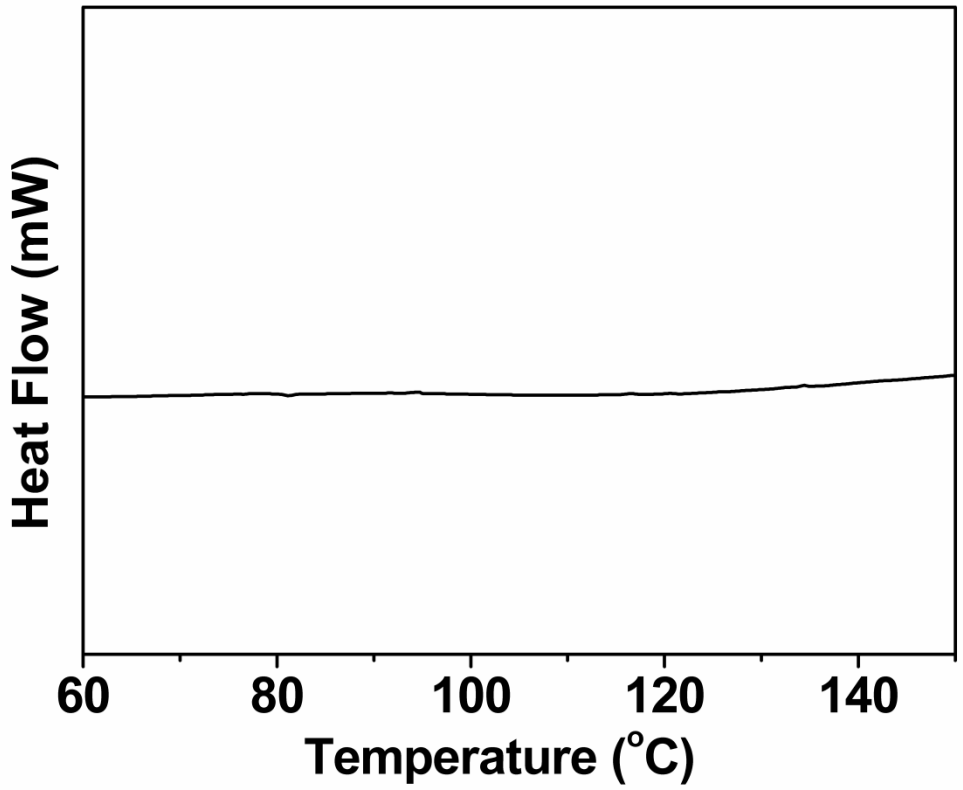

Figure 7 [Kumari, Sasidharan and Bhaumik]

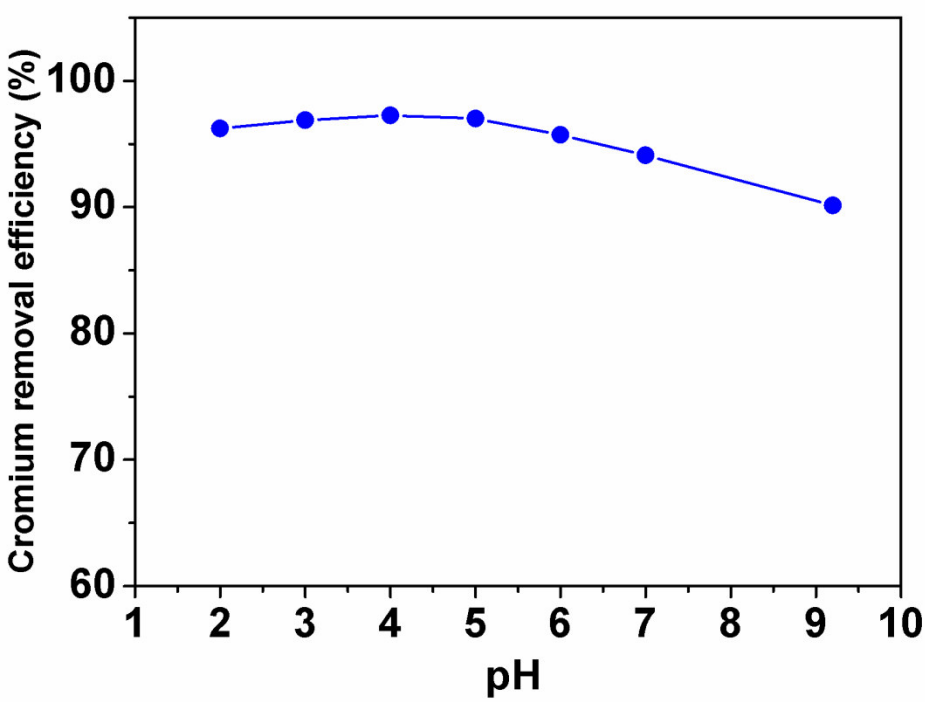

Figure 8 [Kumari, Sasidharan and Bhaumik]

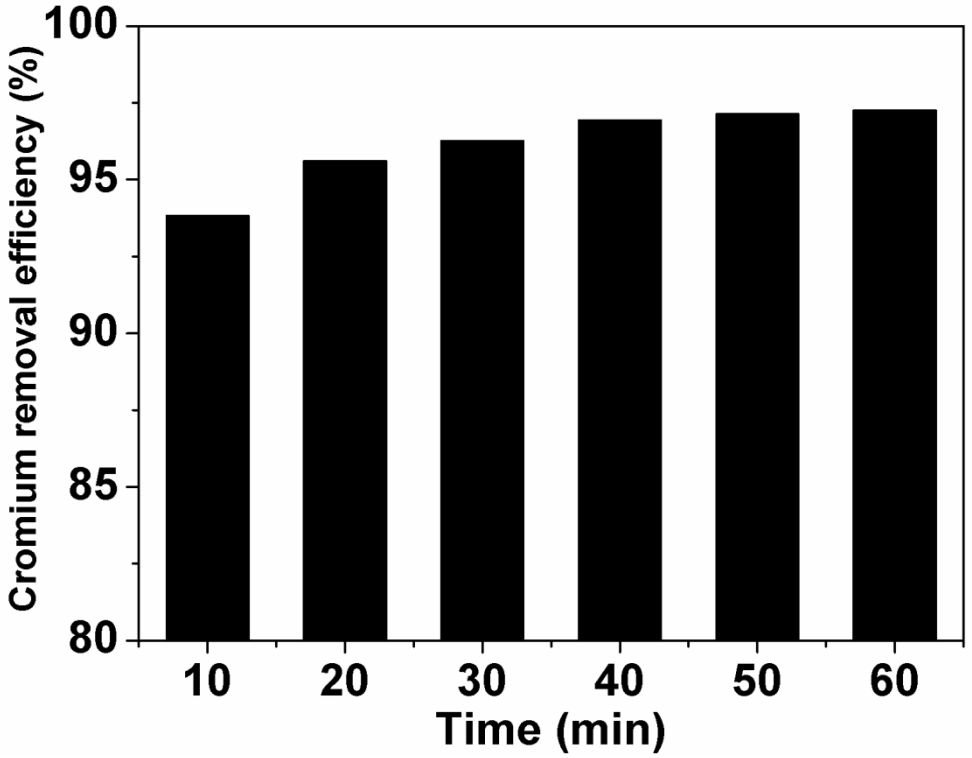

Figure 9 [Kumari, Sasidharan and Bhaumik]

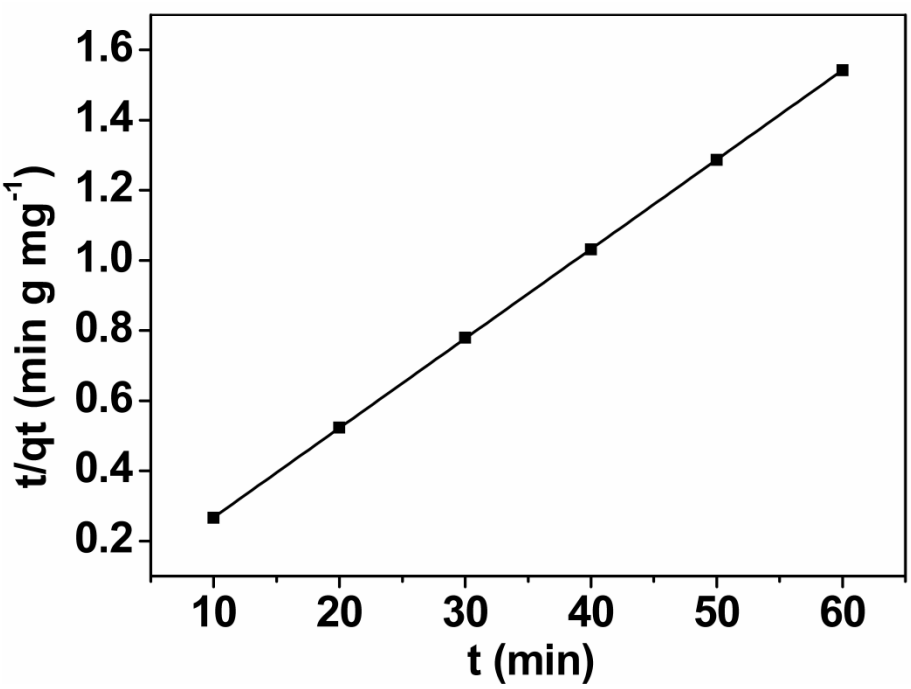

Figure 10 [Kumari, Sasidharan and Bhaumik]

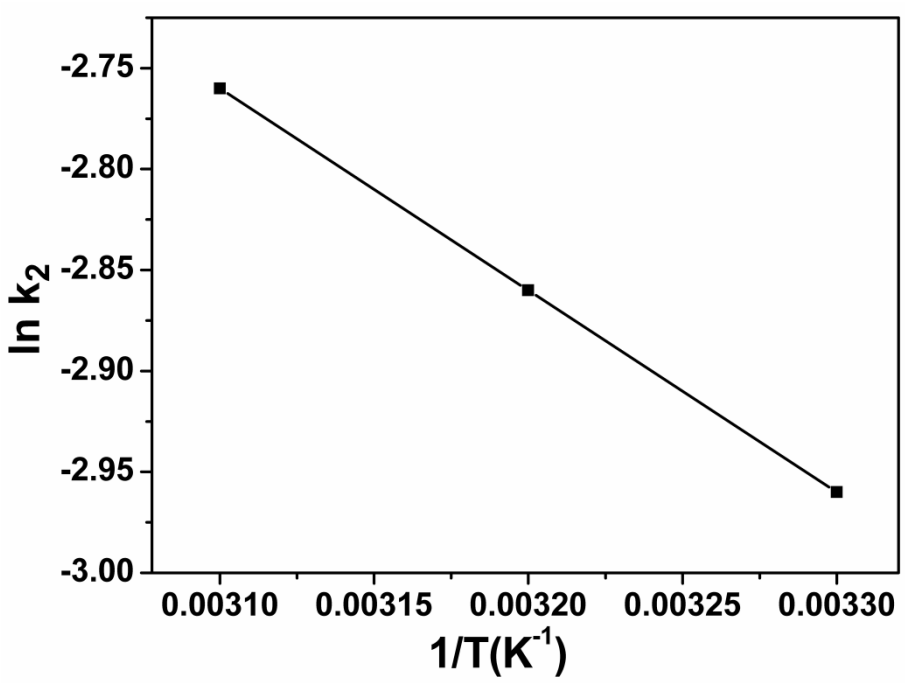

Figure 11 [Kumari, Sasidharan and Bhaumik]